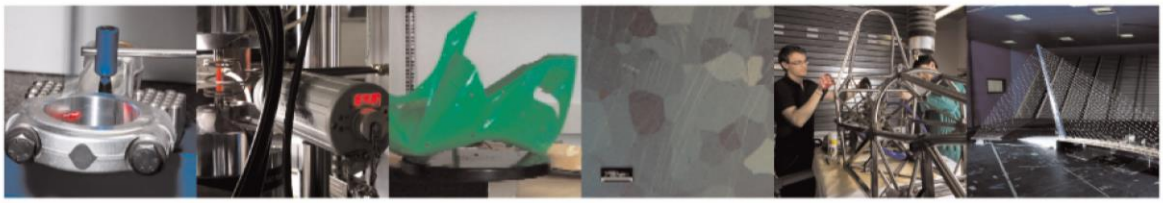

Investigation of remelting and preheating in SLM of 18Ni300 maraging steel as corrective and preventive measures for porosity reduction

Demir, Ali Gökhan; Previtali, Barbara

This is a post-peer-review, pre-copyedit version of an article published in INTERNATIONAL JOURNAL OF ADVANCED MANUFACTURING TECHNOLOGY. The final authenticated version is available online at: http://dx.doi.org/10.1007/s00170-017-0697-z

DIPARTIMENTO DI MECCANICA ■ POLITECNICO DI MILANO
via G. La Masa, 1 ■ 20156 Milano ■ EMAIL (PEC): pecmecc@cert.polimi.it
http://www.mecc.polimi.it
Rev. 0

Investigation of remelting and preheating in SLM of 18Ni300 maraging steel as corrective and preventive measures for porosity reduction

Ali Gökhan Demir*, Barbara Previtali

Department of Mechanical Engineering, Politecnico di Milano, Via La Masa 1, 20156 Milan, Italy

*Corresponding author: aligokhan.demir@polimi.it

Investigation of remelting and preheating in SLM of 18Ni300 maraging steel as corrective and preventive measures for porosity reduction

Ali Gökhan Demir*, Barbara Previtali

Department of Mechanical Engineering, Politecnico di Milano, Via La Masa 1, 20156 Milan, Italy

*Corresponding author: aligokhan.demir@polimi.it

Abstract

One of the most critical defects in selective laser melting (SLM) is the porosity formation. Optimization of process parameters allow for reducing the porosity levels to lower than <1% is possible in most of the cases. Susceptibility to porosity formation can be higher for different alloys as function of chemical composition due to higher spark generation and molten pool instabilities. On the other hand, the probability of porosity formation increases in larger components that due to extended processing time. Powder recoater wear, increase in thermal load, and accumulation of particles in the processing chamber become more relevant as the processing time increases. Hence, the use of integrated monitoring and correction strategies becomes crucially important.

In this work, three different correction strategies are discussed for the correction of porosity during the SLM of 18Ni300 maraging steel. The main aim is the develop a possible correction and prevention scheme to be used within a fully monitored SLM process. The 18Ni300 maraging steel is susceptible to high levels of porosity due to the empirically observed melt-pool instabilities as well as high spark and vapour generation. The correction methods consisted of re-melting of the defected layer employing different scan strategies namely “double-pass”, “soft-melting”, and “polishing”. As a preventive strategy preheating at 170°C was also evaluated. At an initial stage, all the strategies were tested throughout the part built in order to assess their general capacity in improving the part density. Surface roughness, geometrical error and material microhardness were also evaluated to assess the impact of the strategies on the other quality aspects. The results indicate the capacity of improving the part density and reduce the part roughness effectively.

Keywords: Additive manufacturing; porosity; defect correction; defect prevention; surface roughness; geometrical error; microhardness

1. Introduction

Selective laser melting (SLM) is a powder bed fusion (PBF) based additive manufacturing process, which provides several advantages related to the use of lightweight structures, internal channels, undercuts, design flexibility, and reduced time between design to the final product. Due to the high production times and the cost, SLM is a more viable option for single to small lot production, where these new features are exploited to a large extent. Such conditions are commonly found in aerospace, energy, biomedical, and tooling applications. Evidently, defect formation and component failure have harder consequences in the case of high value, single to small lot productions.

One of the key defects in SLM is the porosity formation. Several mechanisms can be involved in the porosity generation, which are in the most generic terms related to insufficient melting, excessive energy input, or powder bed irregularity [1]. For most of the materials processed with SLM, a range of fluence exists, where porosity can be maintained at acceptable levels (<1%). Lower fluences result in lack of fusion, hence unmolten powder particles remain entrapped between different layers. Excessive fluence generates melt pool instabilities, where material is lost due to spatter and high vaporization. The instable melt pool solidifies with an irregular form generating undercuts, where new layer of powder cannot be placed. Powder bed flaws may form also in optimal fluence conditions and are mainly due to the irregularities on the powder recoater [2]. Both the wear on the powder recoater and particles sticking on it can be the cause of an irregular powder bed. This mainly results in the local excess or absence of material, which can induce lack of fusion or melt pool instabilities respectively. The precautions are mainly related to the component design, its orientation on the build plate, and the choice of the recoater material.

In real applications, the component build time can exceed several days. The build sizes can reach the size of the build chamber of industrial systems of today, which vary between 0.01 to 0.06 m^3. In a volume of 10^{-6} m^3, the total length of the scanned tracks can easily reach 3 km. Hence, there is a high probability of defect formation within the process. Moreover, process drifts can occur within the long build time related to contamination of the process chamber and optical elements. Powder recoater

wear is also common in longer builds with both fine and large structures [3]. This can generate local powder bed irregularities resulting in pore formation due to missing material.

The process chamber heats up throughout the process varying the initial melting conditions. All of these conditions can be monitored in-situ [4],[5]. The layer-by-layer building strategy provides the possibility of correcting the defect that forms at a given layer before further processing. This distinct feature of SLM can be beneficial for achieving defect-free components especially for correcting internal defects such as porosity. Despite several developments in the process monitoring field and the intrinsic suitability for correction strategies, no online correction strategy has been applied in literature.

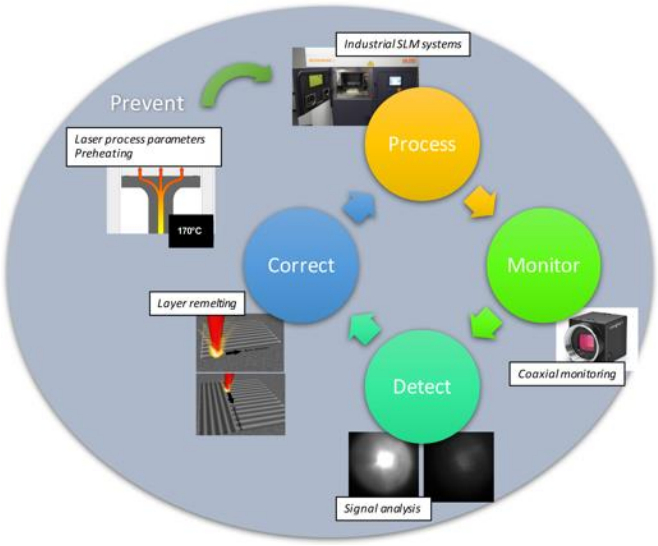

Figure 1. Application of prevention and correction methods in a fully monitored SLM process.

Figure 1 illustrates an ideal SLM environment with in-process monitoring and the use of prevention and correction methods. The prevention methods consist of the use of correct process parameters [6],[7], scan strategies [8],[9], component [10] and support design [11],[12], which are essential features that reduce the probability of defect formation. Once the process is initiated, monitoring equipment should start acquiring data. If a defect is formed, the monitoring system should be able to signal it in due time, and initiate the correction strategy. The use of correction strategies rather than an online process control scheme can be beneficial for SLM process, since the process dynamics can be very fast for controlling the system components in real time.

Concerning the prevention strategies, the use of preheating in SLM has been studied sparingly in literature [13],[14]. Preheating is commonly applied to resolve in-process cracking and thermal distortions due to the fast cooling. It is a common practice in laser cladding of materials with high crack susceptibility [15–17]. In SLM, the use of preheating is limited to relatively lower temperatures in industrial SLM systems (around 200°C). In these conditions, preheating can provide added energy along with the energy provided by the laser beam and it can reduce the porosity formed due to lack-of-fusion [13]. Similarly, the molten pool can be maintained more stable by inducing a slower cooling rate.

Concerning defect correction in SLM two main approaches arise, which use: i) subtractive, and ii) constant volume strategies. The subtractive strategies can involve the use of a secondary laser source for ablation of the previously built layer [18]. There are industrial systems employing milling stations integrated in the build chamber to use a similar approach [19],[20]. The constant volume strategies involve mainly the use of the same laser source for remelting the layer. This solution can be useful for flattening the surface irregularities and especially for porosity reduction. As a matter of fact, remelting passes have been previously applied at the final layer of the built component to improve the surface roughness [21–24].

In this work, prevention and correction strategies are evaluated with on board capabilities available to an industrial system working with pulsed wave (PW) laser emission and preheating up to 170°C (Renishaw AM250). Prevention (i.e. pre-heating) and correction (i.e. re-melting layer by layer during the process) strategies were developed on a 18Ni300 maraging steel. The 18Ni300 maraging steel is a Fe-Ni alloy typically manufactured by block casting, which is followed by a series of forming and machining processes. The manufacturing sequence is followed by the application of the aging treatment, which provides a combination of high strength and ductility by the formation of strengthening precipitates [25]. Such properties render the material highly appealing for the manufacturing of moulds and dies, as well as aerospace and automotive components. The application areas of the material call for a technology suitable for producing complex components in small

quantities in short lead times. SLM technology can meet with such requirements; however, defect generation becomes more critical due to the high value of the product. Moreover, 18Ni300 was observed to be susceptible to porosity formation due to the empirically observed melt-pool instabilities as well as high spark and vapour generation, showing an evident need for porosity reduction [26]. Indeed, in tooling, aerospace, and automotive applications the trace levels of porosity can be detrimental on the fatigue properties. This might lead to a reduction of the number of products producible by the additively manufactured die, or premature failure of the aerospace and automotive components. The paper describes the developed strategies, evaluating their effects on the defect to be corrected, namely porosity, as well as the collateral effects on other quality aspects namely surface roughness, dimensional error, and microhardness.

2. Materials and methods

2.1. Material

A gas atomized 18Ni300 maraging steel powder was used throughout the study (Sandvik Osprey, Neath, UK). Figure 2.a shows the morphology of the used powder. The average particle size was 32.8 μm with D10 and D90 at 19.6 μm and 53.7 μm respectively. The tap density was 5 g/cm$_3$, whereas the nominal material density is 8.1 g/cm$_3$. The nominal chemical composition of the alloy is given in Table 1.

Table 1. Chemical composition of the maraging steel 18Ni300 powder declared by the producer.

Element	Ni	Co	Mo	Ti	Cr	Si	Mn	Al	Cu
wt%	17.6	9.6	5.3	0.7	0.49	0.1	0.1	0.09	0.05

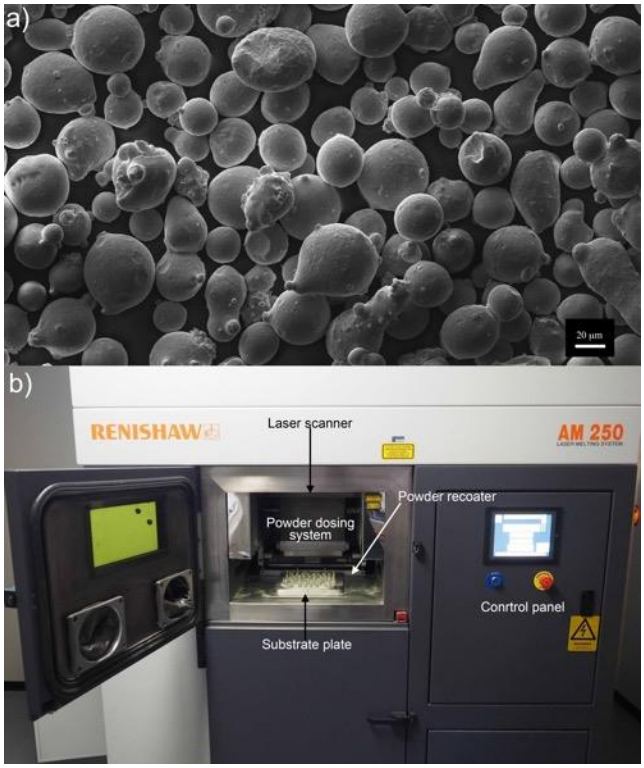

Figure 2. a) Morphology of the 18Ni300 maraging steel powder. b) Details of the Renishaw AM250 system used in the experiments.

2.2. Selective laser melting system

Renishaw AM250 was used throughout the experimental work (Stone, UK). Figure 2.b shows the system in detail. The system implemented a 200 W active fiber laser (R4 from SPI, Southampton, UK). The estimated beam diameter is 75 µm on the focal plane. During the preparation phase, the system applies vacuum the processing chamber down to -950 mbar pressure and then it is flooded with Ar reaching 15 mbar overpressure. Throughout the process the oxygen content of chamber is maintained below 1000 ppm. The system employs pulsed wave (PW) emission. Build plate can be preheated up to 170°C by employing a soaking cycle applied prior to the process. For slicing and post processing of the layer trajectories Magics 19 was used (Materialise, Leuven, Belgium).

2.3. Experimental plan

The present SLM system allowed to control the main process parameters, namely pulse peak power (P_{peak}), pulse duration (t_{on}), point (d_p) and hatch (d_h) distances, focal position (f), and the layer

thickness (z). Experimental conditions were derived from previous work on the same material [26]. The first scanned layer aimed at depositing the material layer, and the second one aimed at porosity correction, which are referred hereafter to as volume and remelting passes respectively. Volume and remelting strategies were designed considering fluence, pulse and line overlaps. Fluence defines the energy density over the scanned area and can be calculated from the following equation.

$$F = \frac{P_{peak} \cdot t_{on}}{d_p \cdot d_h} \quad \text{Eq.(1)}$$

For a given laser beam diameter (d_s), if each pulse is placed with a certain point distance (d_p), pulse overlap can be calculated as:

$$O_p = (d_s - d_p)/d_s \quad \text{Eq.(2)}$$

On the other hand, line overlap (O_l) between consecutive scan lines depends on hatch distance (d_h) and can be calculated as:

$$O_l = (d_s - d_h)/d_s \quad \text{Eq.(3)}$$

Both pulse and line overlap can be negative, if point distance or hatch distance is larger than the beam diameter. It should be noted that molten pool can be larger than the laser beam diameter, hence even with negative pulse or line overlaps continuous molten tracks can be achieved.

In the experimental work, only the pulse duration was varied in the volume pass at 70, 80, and 90 µs. Three different remelting strategies were tested along with the condition without any remelting (none-*N*). The correction strategies based on remelting were namely, double pass (*DP*), soft remelting (*SR*), and polishing (*P*). The remelting strategies are schematically described in Figure 3. The figure schematizes the change in the beam intensity obtained through the change in power levels, the change in pulse and line overlaps, and the size of the laser beam as a function of the applied strategy. In the *DP* strategy, the same scan pattern is applied twice without changing the laser parameters [27]. The *SR* strategy aims to correct zones with incomplete melting by providing lower energy with shorter pulses on the material, and a constant molten track provided by increased pulse overlap. Hence, the *SR* strategy consisted in the use higher pulse overlap and lower line overlap compared to the volume

pass. The *P* strategy aims to provide a larger and shallower molten pool, similar to the conditions used in laser polishing [28],[29]. For the *P* strategy, a defocused beam was employed enlarging the beam diameter to approximately 100 μm on the powder bed. The fluence of *P* was similar to that of *SR* strategy, applied with a higher line overlap. As a preventive measure, preheating was also tested for all combinations. The substrate plate was heated to 170°C prior to the process. The substrate was cooled down by simply turning off the heating system after the end of the build. The duration of each built was approximately 14.5 hours. The experimental plan produced 24 different configurations, which were all replicated 3 times. Two builds were executed with and without the use of preheating, consisting in the blocked factor within the experimental plan. Accordingly, the interaction of this parameter with other was not considered in the analysis. Cylindrical samples with 10 mm diameter and 20 mm height were produced. No beam compensation, contour melting, up or down skin strategies were applied to the geometries. The scan direction was varied by 67° after each layer. The remelting pass was carried out perpendicular to the scan direction of the volume pass. The details of the experimental campaign are shown in Table 2. The parameters corresponding to the different remelting strategies are shown in Table 3.

Table 2. Fixed and varied parameters in the experimental campaign

Fixed parameters	
Laser peak power, P_{peak} (W)	200
Point distance, d_p (μm)	65
Hatch distance, d_h (μm)	90
Focal position, f (mm)	0
Layer thickness, z (μm)	40
Pulse overlap, O_p	13%
Line overlap, O_l	-20%
Varied parameters	
Pulse duration, t_{on} (μs)	70 (F=239 J/cm2), 80 (F=274 J/cm2), 90 (F=308 J/cm2)
Remelting strategy	None, Double pass (*DP*), Soft remelting (*SR*), Polishing (*P*)
Pre-heating	None, 170°C

Table 3. Details of the remelting strategies.

Strategy	P_{peak}(W)	t_{on} (µs)	d_p (µm)	d_h (µm)	f (mm)	O_p	O_l	F (J/cm2)
Double pass, *DP*	Same as the first pass							
Soft remelting, *SR*	150	50	35	100	0	53%	-33%	214
Polishing, *P*	200	85	80	100	-2	20%	0%	213

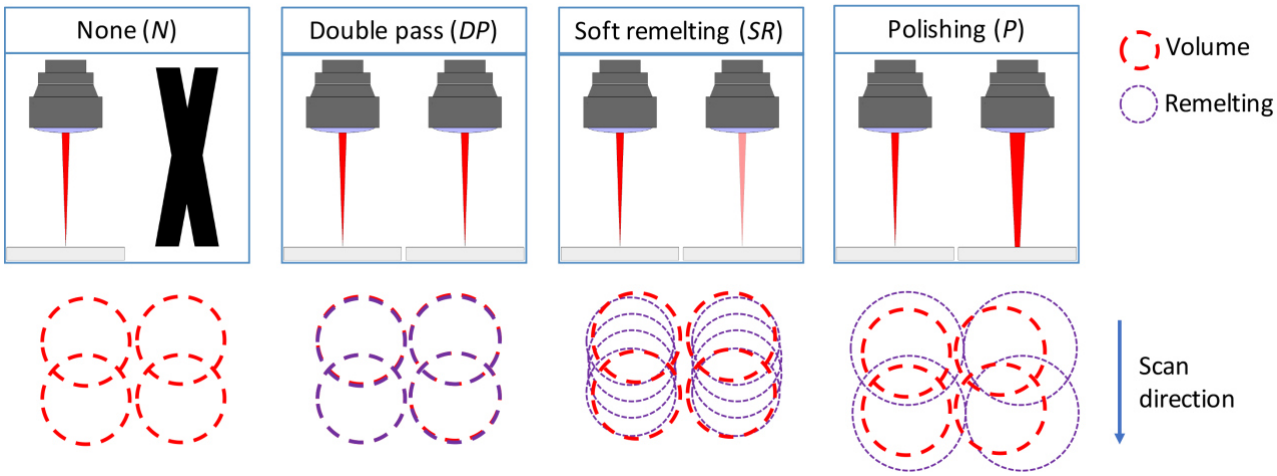

Figure 3. Schematic representation of the volume and remelting passes applied at each strategy.

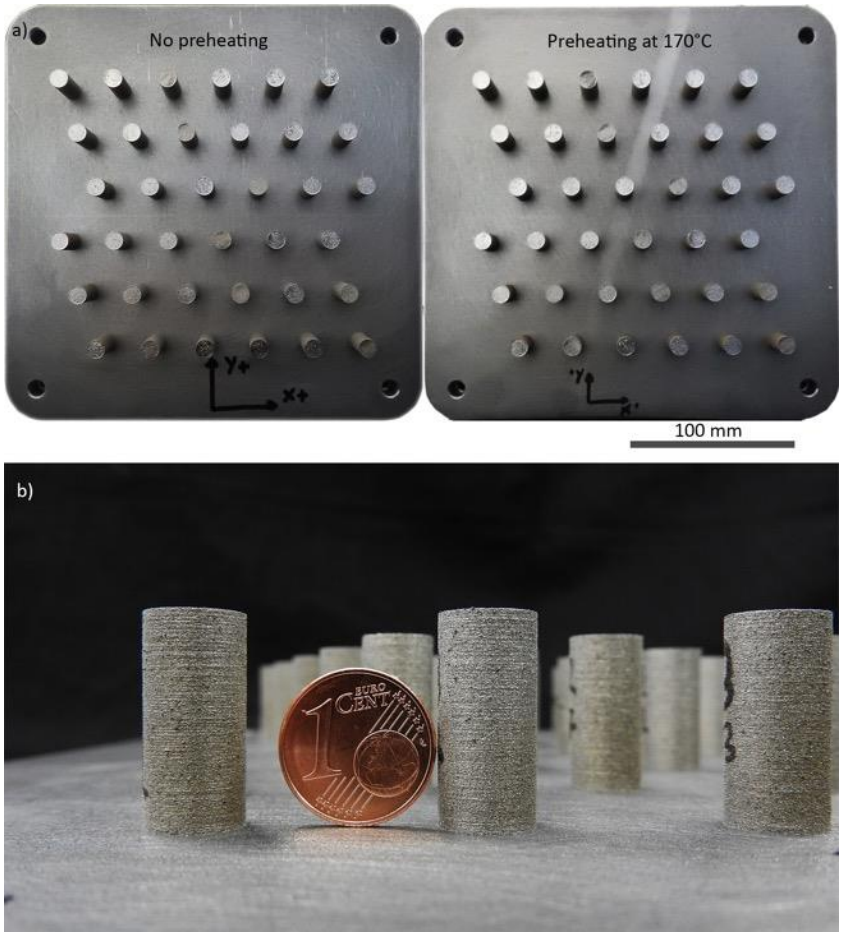

Figure 4. a) Images of the build specimens on the build plates. b) Close-up images of the specimens.

2.4. Characterization

SEM images of all the specimen surfaces were acquired (EVO-50 from Carl Zeiss, Oberkochen, Germany). Average surface roughness (*Sa*) was measured by focus variation microscopy (Infinite Focus from Alicona, Graz, Austria). Acquisitions were made over area of 2.85x2.16 mm^2 with 5X objective over the scan plane (xy) on top of the build specimens. Estimated lateral and axial resolutions were 0.5 μm and 7 μm respectively. Roughness profile was extracted from the acquired profiles employing a short-pass Gaussian with cut-off length at 569 μm. Density (ρ) was measured employing Archimedes method with a precise scale (100-300M from Precisa, Turin, Italy). Metallographic cross-sections of the realized samples were prepared by cutting, mounting in resin and polishing. Optical microscopy images of the cross sections were acquired with 5X objective (Quick Vision ELF from Mitutoyo, Kawasaki, Japan). Dimensional accuracy of the build parts was assessed using coordinate measurement machine (CMM, Prismo 5 VAST MPS HTG from Carl Zeiss, Oberkochen, Germany). Radius deviation was calculated employing the following expression

$$e_r = r_m - r_n \quad \text{Eq.(4)}$$

where r_m is the measured and r_n is the nominal radius (10 mm). Vickers microhardness was measured on all samples, with 2 kgf applied load (VMHT 30A from Leica, Wetzlar, Germany). Five measurements along the radial axis were taken for each condition on the scanned surface plane approximately at 2 mm above the substrate plate. This position was taken in order to evaluate a region that forms in the initial phases of the build, which is far enough from the first few layers, and will remain under the influence of the heat provided by the preheating and the consecutive scanned layers. Material microstructure was analyzed over the same cross-sections after chemical etching with Picral solution. Analysis of variance (ANOVA) was applied to all response variables. The significant parameters were identified with Bonferroni criteria using an overall statistical significance level at 5%. For each analyzed response variable ANOVA composed of 4 statistical tests, hence the statistical

significance of a single parameter or interaction was 1.25%. Residuals were controlled for normality and homogeneity.

3. Results and discussion

Table 4 presents the correlation coefficients between density, radius deviation, and surface roughness. The microhardness could not be evaluated due to the different sample size. The Pearson correlation coefficients depict that the response variables are correlated weakly (<0.5) and inversely (-). This was also verified by the scatter plots of each response variable couple. The overall results highlight that different parameters have different effects on different quality aspects. Consequently, each quality aspect is separately analyzed in the following sections. Results are accompanied by the ANOVA table and the interval plot of the statistically significant parameters with standard error for each group.

Table 4. Correlation between the response variables

Response pair	Pearson correlation
Density (ρ)-Radius deviation (e_r)	(-)0.333
Density (ρ)-Surface roughness (Sa)	(-)0.259
Radius deviation (e_r)- Surface roughness (Sa)	(-)0.244

3.1. Surface morphology

Figure 5 gathers the SEM images of the surfaces belonging to each parameter combination. Surface morphology is an important indicator for the porosity formation both due to lack of fusion and melt pool instability [30]. It can be seen that between preheating conditions there is not a significant difference in appearance. On the other hand, a remarkable change is visible between the different remelting conditions, whereas the effect of pulse duration seems to be limited. The surfaces after the single volume pass (N) appear to be highly irregular and are composed of several voids and protrusions. The voids are starting conditions for porosity formation, which can be possibly filled in

by the newly deposited powder layer. On the other hand, the protruded regions may generate undercuts, where the new powder layer cannot penetrate into. The surface voids tend to reduce with increased pulse duration. The application of a remelting pass with the same process parameters as the volume pass (*DP*) tends to produce a relatively more homogenous surface with reduced voids. Protruded and undercut regions still appear when higher pulse durations are used. The use of the *SR* strategy proves to provide sufficient remelting over the scanned line, since smooth melt tracks are visible produced by the high pulse overlap. This strategy produces a new surface texture composed of micro voids generated between the molten tracks due to an insufficient line overlap. The use of higher pulse duration provides improvements in terms of reducing these micro voids. The *P* strategy produces large melt tracks over the surface generating overall a smooth surface texture. Combined with the highest pulse duration at the volume scan, the *P* strategy provides a flat surface implying a lower porosity and a better surface finish.

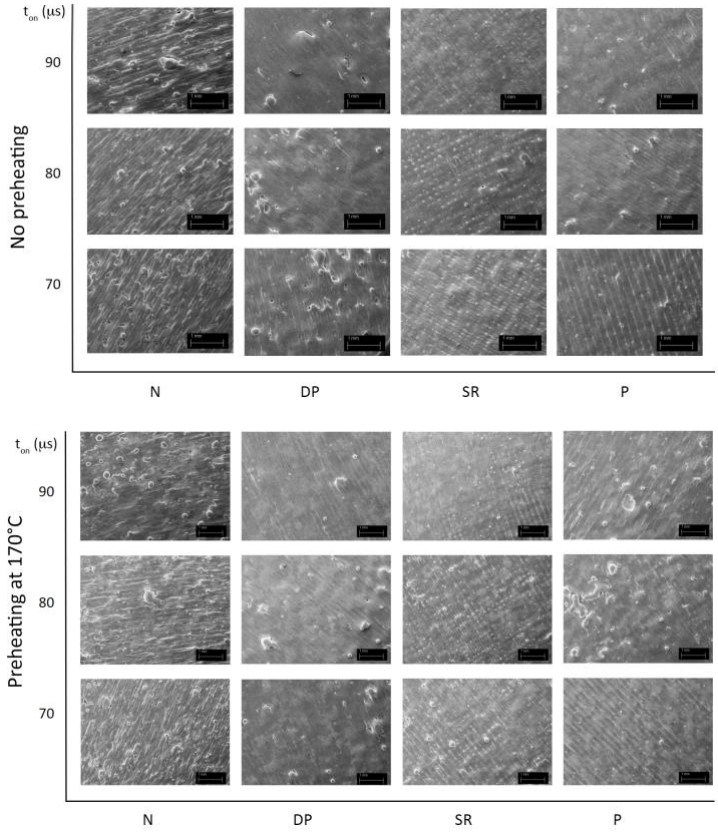

Figure 5. Surface morphology of SLM produced 18Ni300 maraging steel samples as a function of process parameters. Images show the last scanned layer on top of the specimens.

3.2. Density

As indicated in Table 5, the only statistically significant parameter over the part density is the remelting strategy. The low R^2_{adj} value indicates unexplained variability in the results. This is expected to be due to the fact that over the experimented region the measured densities are close to the full density and the variations induced by the processing strategies are limited with respect to the natural variability of the process. It should be noted that the even small increments are appreciable in the final applications. Such improvement in material density is more evident in the micrographs depicted in Figure 6. It can be seen that the lowest part density is achieved without any remelting (*N*). All remelting strategies provide a degree of improvement over the density, where the performance increases from *DP* to *SR,* and *P* is the best strategy. These results are coherent with the surface morphology observations. As seen in the cross-section images in Figure 7, the porosity levels are low already without any remelting (*N*). However, these remaining local defects which, range between 20-200 μm in size are the ones that require correction in order to ensure the required performance especially under fatigue conditions. It can be seen that defect free parts can be achieved applying the correct remelting strategy. As ANOVA depicts, there is no statistical significance of preheating, which declines the possibility of using this technique as a preventive measure.

Table 5. ANOVA table for density (ρ).

Source	*DF*	*Adj SS*	*Adj MS*	F-value	P-value
Preheating	1	0.00892	0.000892	2.87	0.096
Remelting	3	0.005166	0.001722	5.54	0.002
t_{on}	2	0.001386	0.000693	2.23	0.117
Remelting* t_{on}	6	0.003413	0.000586	1.88	0.099
Error	58	0.018039	0.000311	0.33	
Total	70	0.029044			
S=0.0176359		R^2=37.89%		R^2_{adj}=25.04%	

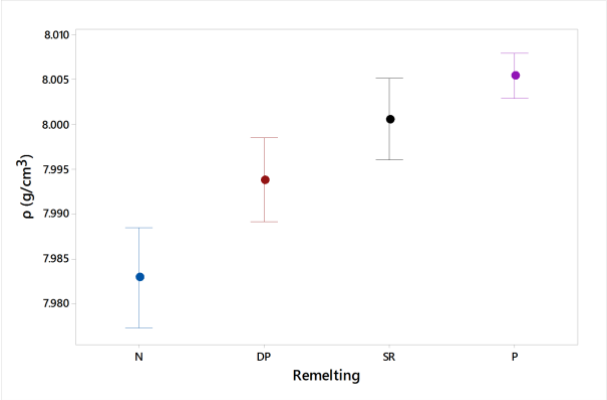

Figure 6. The effect of remelting strategies on part density.

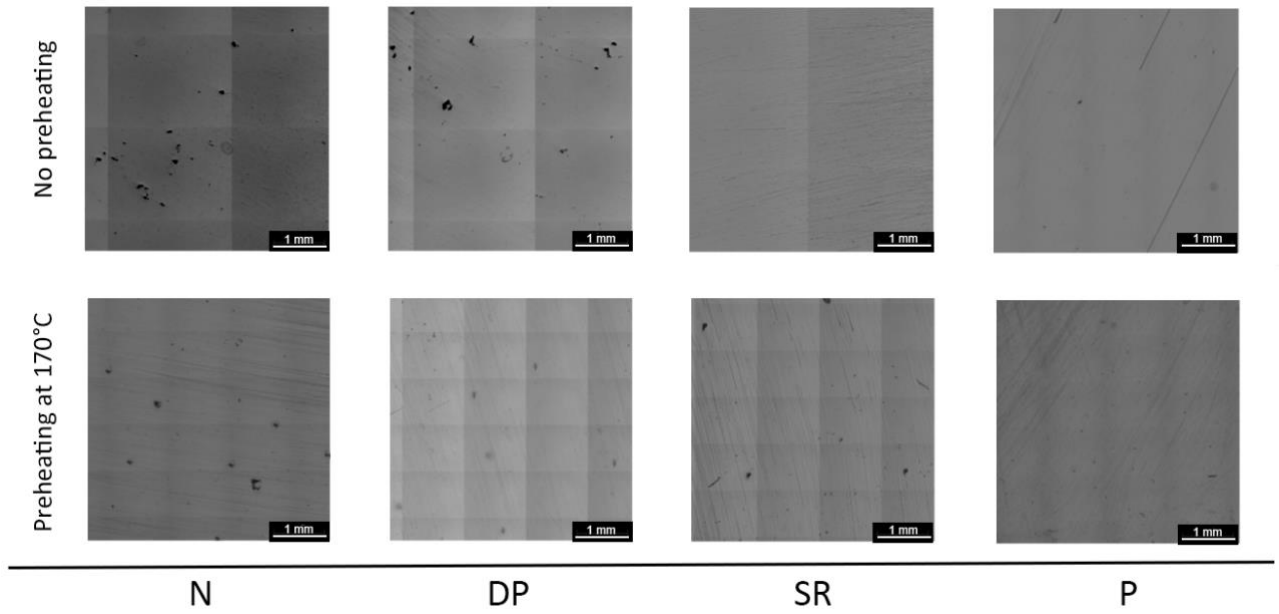

Figure 7. Transversal cross-sections of the specimens taken along the scan plane (xy) showing porosity as a function of preheating and remelting conditions (t_{on}=80 µs).

3.3. Surface roughness

The statistical analysis showed that remelting and pulse duration are the influential parameters over the average surface roughness (see Table 6). Figure 8 shows the effect of the significant parameters. It can be seen that surface roughness is lowered by all of the remelting strategies, where *DP* and *P* show the smallest roughness overall. The use of high pulse duration at the volume pass also improves the surface finish. Combined together high pulse duration (90 µs) and the use of *DP* or *P* strategies can lower the average surface roughness to approximately 4 µm, which corresponds to a 50% reduction compared to the surface without any remelting (*N*, t_{on}=90 µs). The combined effect of

higher pulse duration and remelting strategies can be attributed to an improved efficacy of the remelting strategy starting from a surface with a smaller amount of defect. With lower pulse durations, the remelting pass can be also influential on closing subsurface defects or defects remaining from the previous layer. With less amount of subsurface defects the remelting pass is expected to have a corrective effect on the final layer providing a smoother finish.

Figure 9 reports the surface height maps acquired by the focus variation microscope. The images point out a highly irregular surface texture achieved without any remelting. There are several surface pits as also observed in the SEM images, and the peak to valley difference can be as high as 260 µm in the worst condition (*N*, t_{on}=70 µs). The use of remelting strategies eliminates most of these surface irregularities. However, in particular the *SR* strategies generates an underlying new surface texture also observed in the SEM images, which induces a more regular, yet rough surface. The main difference between the *DP* and *P* strategies appears as the surface homogeneity, which is not easily captured by the average surface roughness parameter *Sa*.

Table 6. ANOVA table for average surface roughness ($Sa_{-0.5}$).

Source	*DF*	*Adj SS*	*Adj MS*	F-value	P-value
Preheating	1	0.004365	0.004365	2.15	0.148
Remelting	3	0.119854	0.039951	19.64	0.000
t_{on}	2	0.030019	0.015009	7.83	0.001
Remelting* t_{on}	6	0.022597	0.003766	1.85	0.105
Error	59	0.120029	0.002034		
Total	71	0.296863			
S=0.0451043		R_2=59.57%		R_{2adj}=51.34%	

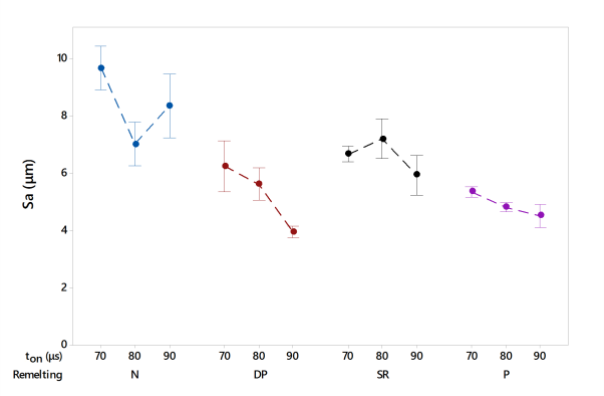

Figure 8. Effects of pulse duration and remelting strategies on surface roughness. Connection lines depict trend only.

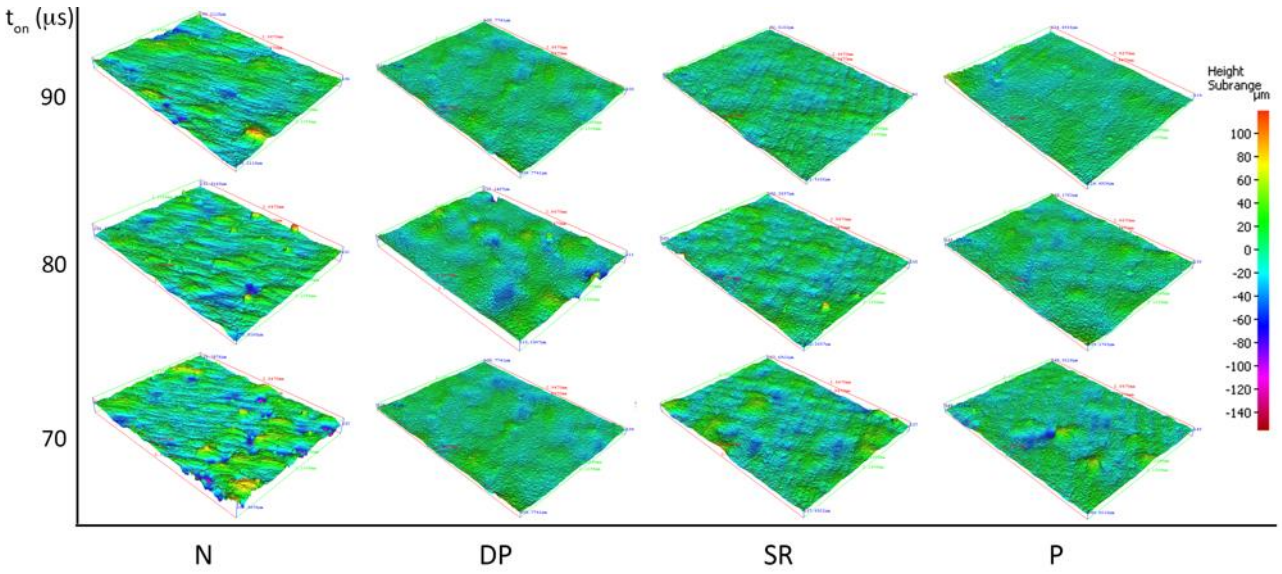

Figure 9. Height maps of the different surface conditions as a function of pulse duration and remelting strategy (no preheating applied).

3.4. Geometrical error

The statistical analysis shows that all three process parameters have significant effects on the radius deviation without the interaction between remelting and pulse duration (see Table 7). Figure 10 shows the effect of each process parameter on radius deviation. It was seen that the main effect of both pulse duration and preheating was an increase on the dimensional error. On the other hand, compared to a single pass strategy (*N*) the error is increased increasingly following the order of *SR*, *P*, and *DR*. The changes induced by the pulse duration and the remelting strategies can be directly linked to an increase of the melt pool. The influence of preheating can be related to an increase of the melt track due to the added energy provided by the higher initial temperature [13], as well as to an increase of diameter by the sintered particles. It should be noted that no surface finishing operation was carried out on the specimens. As a matter of fact, the use of preheating induces a mean increase of 30 µm in the geometrical error. Such dimension is comparable to the average particle size of the powder. The operational implication of these result is that the beam compensation should be adapted to used configuration. The results also show that a larger molten and resolidified track, which can be approximated by the dimensional error, does not necessarily provide a higher density. As a matter of

fact, the density measurements showed the influence of the remelting strategy only, where the best conditions (*P*) does not correspond to the highest average radius enlargement.

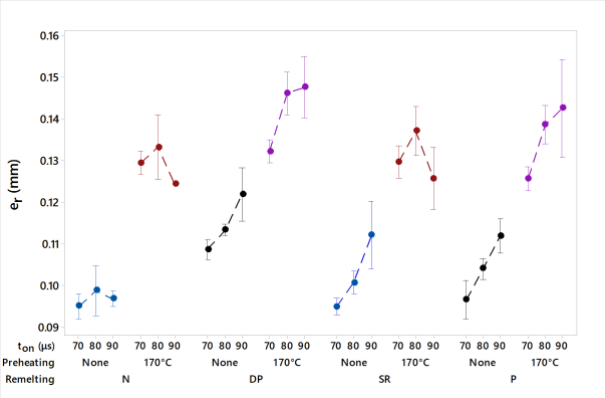

Figure 10. Effects of process parameters on radius deviation. Connection lines depict trend only.

Table 7. ANOVA table for radius deviation (e_r).

Source	*DF*	*Adj SS*	*Adj MS*	F-value	P-value
Preheating	1	0.016040	0.016040	204.54	0.000
Remelting	3	0.002319	0.000773	9.86	0.000
t_{on}	2	0.001089	0.000544	6.94	0.002
Remelting* t_{on}	6	0.000620	0.000103	1.32	0.264
Error	59	0.004627	0.000078		
Total	71	0.024695			
S=0.0088555		R^2=81.26%		R^2_{adj}=77.45%	

3.5. Microhardness

The statistical analysis showed that microhardness is affected by remelting and preheating, and the interaction between pulse duration and remelting (see Table 8). Figure 11 shows the effect of process parameters on the Vickers microhardness. Evidently, the highest impact derives from the preheating, which generates a mean reduction of 40 HV. The influence of remelting strategies is much more restricted as there is an average reduction of approximately 5 HV between the condition with the highest (*N*) and lowest hardness (*SR*). The 18Ni300 maraging steel is a material designed for a specific heat treatment. Commonly, the maraging steel components undergo a solution annealing to homogenize the microstructure prior to the aging treatment. Evidently the thermal history of the material can induce difference in the outcome of the successive heat treatments [25]. A standard solution annealing applied at 815°C for 30 minutes on the SLM produced specimens reduces the

hardness to around 280 HV [31]. The production of specimens took around 7 hours of build time. The reduction in the material hardness is expected to be due to a slight coarsening of the microstructure. As shown in Figure 12, all conditions without preheating produce fine microstructure, where a slight coarsening is observable with *SR* condition. Preheating generates coarser microstructure on all the specimen types with a mixed appearance of cellular and dendritic structures. The *SR* condition, which is characterized by the lowest microhardness, exhibits larger grains.

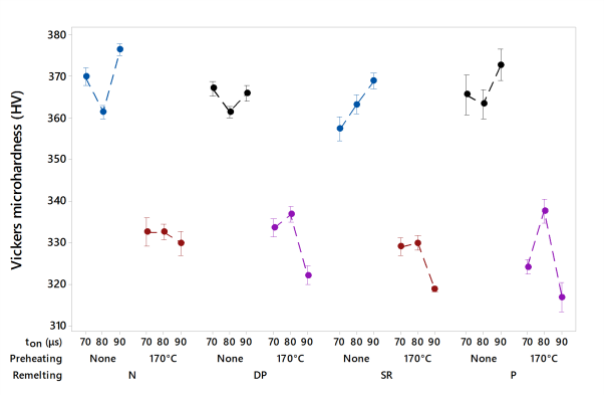

Figure 11. Effects of process parameters on Vickers microhardness. Connection lines depict trend only.

Table 8. ANOVA table for Vicker microhardness.

Source	*DF*	*Adj SS*	*Adj MS*	F-value	P-value
Preheating	1	37130.9	37130.9	796.35	0.000
Remelting	3	559.8	186.6	4.00	0.010
t_{on}	2	68.7	34.3	0.74	0.481
Remelting* t_{on}	6	709.3	118.2	2.54	0.025
Error	97	4522.7	46.6		
Total	109	44000.9			
S=0.0088555		R_2=81.26%		R_{2adj}=77.45%	

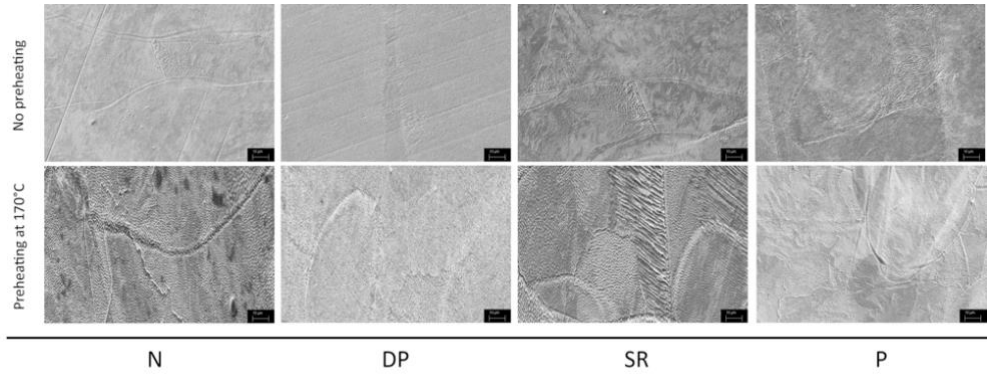

Figure 12. Cross-sections of the specimens showing the material microstructure as a function of preheating and remelting conditions.

4. Conclusions

In this work, the use of remelting and preheating was evaluated for possible correction and prevention techniques to reduce porosity in selective laser melting. The 18Ni300 maraging steel was the tested material, which is known to possess low processability with SLM using PW laser emission. The use of PW laser emission and the intrinsic sensitivity of the processed material to heat constituted further constraints on the tested methods. In the scheme of a monitored process the use of correction strategies should be applied on demand and where required in order to reduce the impact on increased process time. The choice of the optimal correction strategy relies on the evaluation of the corrected defect (porosity) as well as the possible collateral effects due to the use of the strategy. The main results of this work are as follows.

- The remelting strategies are effective in improving the part density, where the strategy based on a superficial melting, namely polishing (*P*), proved to be best solution. The polishing strategy provided a smooth surface free of pits and protruded zones inherent from the initial volume melting pass.
- Surface roughness and part density are closely linked to each other. The results depict that surface smoothing provided by the remelting pass is highly beneficial for preventing the pore formation and propagation through the layers.
- Preheating of the 18Ni300 maraging steel provided no improvement in the part density and hence fails as a preventive measure. It induced larger dimensional error presumably due to the sintering of the powder particles, and lower microhardness expected to be due to an in-process annealing action.
- All remelting strategies induced higher dimensional error, linked to the enlargement of the melt pool. If applied only on the zone where correction is required, the remelting strategies are not expected to induce any dimensional errors. If the correction strategy is to be applied through the complete layer, beam compensation should be adjusted differently.

- The remelting strategies influence the material microstructure and induce slight grain coarsening. If the correction strategies are applied only at the correction zone, such differences are not expected to be influential on the mechanical behaviour. The influence of remelting applied at every layer on the heat treatment outcome requires further attention.

Besides the general outcomes, the present work illustrates a generic method to evaluate the effects of possible corrections strategies in SLM on different quality factors. The use of remelting is an appealing option, since it is based on the same laser source used for producing the component. However, the strategy should be developed for the given material. In this work, the remelting strategies development was based on literature survey and previous experience. The implementation of modeling and simulation tools can be highly beneficial in future to reduce the amount of iterative and extensive experimental work.

Acknowledgements

The authors wish to express their gratitude Mr. Matteo Bozzani and Mr. Davide Beretta for their contribution to the experimental work. This work was supported by Regione Lombardia under the call “Creatività: Eventi e Luoghi per L’innovazione nella Moda e nel Design, Linea 2: Infrastrutturazione Fisica e Digitale” and the project MADE4LO under the call "POR FESR 2014-2020 ASSE I - AZIONE I.1.B.1.3”.

References

[1] Gong H, Rafi K, Gu H, Starr T, Stucker B. Analysis of defect generation in Ti-6Al-4V parts made using powder bed fusion additive manufacturing processes. Addit Manuf 2014;1:87–98. doi:10.1016/j.addma.2014.08.002.

[2] Abdelrahman M, Reutzel EW, Nassar AR, Starr TL. Flaw detection in powder bed fusion using optical imaging. Addit Manuf 2017;15:1–11. doi:10.1016/j.addma.2017.02.001.

[3] Neef A, Seyda V, Herzog D, Emmelmann C, Schönleber M, Kogel-Hollacher M. Low coherence interferometry in selective laser melting. Phys Procedia 2014;56:82–9. doi:10.1016/j.phpro.2014.08.100.

[4] Everton SK, Hirsch M, Stravroulakis P, Leach RK, Clare AT. Review of in-situ process monitoring and in-situ metrology for metal additive manufacturing. Mater Des 2016;95:431–45. doi:10.1016/j.matdes.2016.01.099.

[5] Grasso M, Colosimo BM. Process defects and *in situ* monitoring methods in metal powder bed fusion: a review. Meas Sci Technol 2017;28:44005. doi:10.1088/1361-6501/aa5c4f.

[6] Kasperovich G, Haubrich J, Gussone J, Requena G. Correlation between porosity and processing parameters in TiAl6V4 produced by selective laser melting. Mater Des 2016;105:160–70. doi:10.1016/j.matdes.2016.05.070.

[7] Kamath C, El-dasher B, Gallegos GF, King WE, Sisto A. Density of additively-manufactured, 316L SS parts using laser powder-bed fusion at powers up to 400 W. Int J Adv Manuf Technol 2014:65–78. doi:10.1007/s00170-014-5954-9.

[8] Aboulkhair NT, Everitt NM, Ashcroft I, Tuck C. Reducing porosity in AlSi10Mg parts processed by selective laser melting. Addit Manuf 2014;1:77–86. doi:10.1016/j.addma.2014.08.001.

[9] Senthilkumaran K, Pandey PM, Rao PVM. Influence of building strategies on the accuracy of parts in selective laser sintering. Mater Des 2009;30:2946–54. doi:10.1016/j.matdes.2009.01.009.

[10] Bouwer S. Leveraging Geometry Optimization Tools to Reduce Component Weight , Development Cost , and Design Schedule Philadelphia , PA. AHS Int 72nd Annu Forum 2016:1–20.

[11] Cloots M, Spierings AB, Wegener K. Assessing new support minimizing strategies for the additive manufacturing technology SLM. Int Solid Free Fabr Symp An Addit Manuf Conf August 12-14 2013 2013:131–9. doi:10.1017/CBO9781107415324.004.

[12] Calignano F. Design optimization of supports for overhanging structures in aluminum and titanium alloys by selective laser melting. Mater Des 2014;64:203–13. doi:10.1016/j.matdes.2014.07.043.

[13] Yadroitsev I, Krakhmalev P, Yadroitsava I, Johansson S, Smurov I. Energy input effect on morphology and microstructure of selective laser melting single track from metallic powder. J Mater Process Technol 2013;213:606–13. doi:10.1016/j.jmatprotec.2012.11.014.

[14] Buchbinder D, Meiners W, Pirch N, Wissenbach K, Schrage J. Investigation on reducing distortion by preheating during manufacture of aluminum components using selective laser melting. J Laser Appl 2014;26:12004. doi:10.2351/1.4828755.

[15] Zhou S, Huang Y, Zeng X, Hu Q. Microstructure characteristics of Ni-based WC composite coatings by laser induction hybrid rapid cladding. Mater Sci Eng A 2008;480:564–72. doi:10.1016/j.msea.2007.07.058.

[16] Zhou S, Zeng X, Hu Q, Huang Y. Analysis of crack behavior for Ni-based WC composite coatings by laser cladding and crack-free realization. Appl Surf Sci 2008;255:1646–53. doi:10.1016/j.apsusc.2008.04.003.

[17] Zarini S, Previtali B, Vedani M, Rovatti L. Cracks susceptibility elimination in fiber laser cladding of Ni-based alloy with addition of tungsten carbides. Proc. ASME 2014 12th Bienn. Conf. Eng. Syst. Des. Anal. ESDA2014, 2014, p. ESDA2014-20623.

[18] Yasa E, Kruth JP. Investigation of laser and process parameters for Selective Laser Erosion. Precis Eng 2010;34:101–12. doi:10.1016/j.precisioneng.2009.04.001.

[19] MC Machinery Systems Inc, Lumex Avance 25 n.d. https://www.mcmachinery.com/products-and-solutions/lumex-avance/ (accessed March 2, 2017).

[20] Sodick Co Ltd, OPM350L n.d. http://www.sodick.jp/product/tool/metal_3d_printer/index.html (accessed March 2, 2017).

[21] Kruth J-P, Yasa E, Deckers J. Roughness improvement in selective laser melting. Proc 3rd Int Conf Polym Mould Innov 2008:170–83.

[22] Vaithilingam J, Goodridge RD, Hague RJM, Christie SDR, Edmondson S. The effect of laser remelting on the surface chemistry of Ti6al4V components fabricated by selective laser melting. J Mater Process Technol 2016;232:1–8. doi:10.1016/j.jmatprotec.2016.01.022.
[23] Kruth J, Badrossamay M, Yasa E, Deckers J, Thijs L, Humbeeck J Van. Part and material properties in selective laser melting of metals. 16th Int Symp Electromachining 2010:1–12.
[24] Yasa E, Kempen K, Kruth J. Microstructure and mechanical properties of Maraging Steel 300 after selective laser melting. Proc 21st Int Solid Free Fabr Symp 2010:383–96.
[25] Jägle EA, Choi P-P, Humbeeck J Van, Raabe D. Precipitation and austenite reversion behavior of a maraging steel produced by selective laser melting. J Mater Res 2014;29:2072. doi:10.1557/jmr.2014.204.
[26] Demir AG, Colombo P, Previtali B. From pulsed to continuous wave emission in SLM with contemporary fiber laser sources: effect of temporal and spatial pulse overlap in part quality. Int J Adv Manuf Technol 2017. doi:10.1007/s00170-016-9948-7.
[27] Zhou X, Liu X, Zhang D, Shen Z, Liu W. Balling phenomena in selective laser melted tungsten. J Mater Process Technol 2015;222:33–42. doi:10.1016/j.jmatprotec.2015.02.032.
[28] Lamikiz A, Sánchez JA, López de Lacalle LN, Arana JL. Laser polishing of parts built up by selective laser sintering. Int J Mach Tools Manuf 2007;47:2040–50. doi:10.1016/j.ijmachtools.2007.01.013.
[29] De Giorgi C, Furlan V, Demir AG, Tallarita E, Candiani G, Previtali B. Laser micropolishing of AISI 304 stainless steel surfaces for cleanability and bacteria removal capability. Appl Surf Sci 2017;406:199–211. doi:10.1016/j.apsusc.2017.02.083.
[30] Qiu C, Panwisawas C, Ward M, Basoalto HC, Brooks JW, Attallah MM. On the role of melt flow into the surface structure and porosity development during selective laser melting. Acta Mater 2015;96:72–9. doi:10.1016/j.actamat.2015.06.004.
[31] Casati R, Lemke JN, Tuissi A, Vedani M. Aging behaviour and mechanical performance of 18-Ni 300 steel processed by selective laser melting. Metals (Basel) 2016;6. doi:10.3390/met6090218.

List of figures

Figure 1. Application of prevention and correction methods in a fully monitored SLM process.

Figure 2. a) Images of the build specimens on the build plates. b) Close-up images of the specimens.

Figure 3. Surface morphology of SLM produced 18Ni300 maraging steel samples as a function of process parameters.

Figure 4. The effect of remelting strategies on part density.

Figure 5. Cross-sections of the specimens showing porosity as a function of preheating and remelting conditions (ton=80 □s).

Figure 6. Effects of pulse duration and remelting strategies on surface roughness.

Figure 7. Height maps of the different surface conditions as a function of pulse duration and remelting strategy

Figure 8. Effects of process parameters on radius deviation.

Figure 9. Effects of process parameters on Vickers microhardness.

Figure 11. Cross-sections of the specimens showing the material microstructure as a function of preheating and remelting conditions.

List of tables

Table 1. Fixed and varied parameters in the experimental campaign

Table 2. Details of the remelting strategies.

Table 3. Summary of ANOVA tests on different response variables.